Size-controlled electrodeposition of Cu nanoparticles on gas diffusion electrodes in methanesulfonic acid solution

Size-controlled electrodeposition of Cu nanoparticles on gas diffusion electrodes in methanesulfonic acid solution

L. Pacquets[a,b], E. Irtem[a], S. Neukermans[a], N. Daems[a,c], S. Bals[b] and T. Breugelmans[a,c]

[a] *ELCAT, University of Antwerp, Universiteitsplein 1, 2610 Wilrijk*

[b] *EMAT, University of Antwerp, Groenenborgerlaan 171, 2020 Antwerpen*

[c] *VITO, Separation & Conversion Technologies, Boeretang 200, 2400 Mol, Belgium*

Corresponding authors: tom.breugelmans@uantwerpen.be

Lien Pacquets ORCID: 0000-0001-9457-685X

Abstract
In this paper electrodeposition is used to obtain Cu nanoparticles, as it allows good control over particle size and distribution. These Cu particles were deposited onto a gas diffusion electrode which increased the resulting surface area. Prior to deposition, the surface was pre-treated with NaOH, HNO_3, MQ and TX100 to investigate the influence on the electrodeposition of Cu on the gas diffusion electrode (GDE). When using HNO_3, the smallest particles with the most homogeneous distribution and high particle roughness were obtained. Once the optimal substrate was determined, we further demonstrated that by altering the electrodeposition parameters, the particle size and density could be tuned. On the one hand, increasing the nucleation potential led to a higher particle density resulting in smaller particles because of an increased competition between particles. Finally, the Cu particle size increased when applying a greater growth charge and growth potential. This fundamental study thus opens up a path towards the synthesis of supported Cu materials with increased surface areas, which is interesting from a catalytic point of view. Larger surface areas are generally correlated with a better catalyst performance and thus higher product yields. This research can contributed in obtaining new insides into the deposition of metallic nanoparticles on rough surfaces.

Keywords
Cu, nanoparticles, dual pulse electrodeposition, Scharifker-Hills model, gas diffusion electrodes

1 Introduction

During the last few decades, nanotechnology has received great attention because of the altered properties of nanoparticles (NPs) compared to their bulk metals [1–4]. When bulk materials are downsized to the nanometer range, it is known that atoms in these NPs behave differently from those present in bulk metals, leading to altered properties compared to the corresponding bulk metals [5]. The use of NPs often leads to an increase in activity and changes in selectivity[2, 5]. Metallic NPs have diverse applications such as electronics and IT [6], medical and healthcare [7]. With this in mind, Cu NPs gained great interest because of their high electrical conductivity, low electrochemical migration behavior, low material cost and interesting behavior in CO_2 reduction [5, 8–10].

Despite the amount of research concerning the synthesis of Cu catalysts, major challenges remain. For example, Cu NPs can exhibit different facets, leading to different activities [11]. Furthermore, copper has a strong tendency to form various species of oxides when exposed to air [10], [11] which makes it difficult to predict the exact final composition of the catalyst, as its oxidation state varies, which makes it far from straightforward to link the properties to a certain oxidation state. Finally, also the morphology and shape are of utmost importance, as they result in shifts in activity and selectivity [12–14].

Amongst others, synthesis of Cu NPs by electrodeposition is a promising method as a low-cost and large-area growth technique operating at ambient conditions. Electrodeposition is a technique that has drawn a lot of attention because it enables control over the synthesis process, which is a key factor in catalyst optimization. Using this approach, one or more negative potentials are applied in order to reduce the Cu ions, in the electrolyte solution, into Cu metal on the substrate. By slightly changing the applied potential, the particle size and distribution can be tuned leading to changes in activity and selectivity of the catalyst.

In addition to the deposition method, the nature and the structure of the support play an important role in determining the morphology of the nanoparticles. Most of the literature reports the use of glassy carbon electrodes as support for copper electrodeposition [15–18]. However, for industrial applications (e.g. fuel cells [19] or biosensors [20]), a popular approach is to replace GC electrodes with gas diffusion electrodes (GDE) [19–26]. The advantage of using GDEs instead of glassy carbon relies on its large resulting surface area because deposition inside the carbon paper is also possible. However, because of the rough surface of the GDE, we experienced that the deposition of particles is hard to control. In most cases, Cu is spray-painted onto the GDE using binders, which often results in the encapsulation of the particles in the binder with consequent activity losses or poisoning of the catalytic sites (by halides or sulfides). In order to obtain Cu nanoparticles that are well-bond to the surface of the support, electrodeposition represents the optimal solution, as it does not require binders which leads to loss of material. Different groups [21, 22, 25] have deposited Cu on GDE with a single-pulse electrodeposition technique. Unfortunately, this technique allows to obtain particles within a broad size range but the particle size distribution is hard to control because of continuous nucleation. Here we will use dual pulse deposition for the synthesis of Cu on GDE. This approach will enable us to obtain particles with a narrow size distributions on rough surfaces, which can then be applied for various applications (e.g. electronic and optical devices and catalysis [8, 26]).

Since, GDEs are very hydrophobic a pre-treatment is necessary to enable optimal deposition of Cu at its surface. Therefore, extreme operating conditions such as boiling carbon fibers in concentrated HNO_3, a combination of HNO_3 and H_2SO_4 or HCl and HF have been commonly adopted [1, 27–29]. Another widely used pre-treatment is an alkaline treatment with NaOH [29, 30]. The disadvantage of these extreme conditions is that, when used on carbon paper, the paper structure gets partially destroyed. In literature it is already known that the structure of the

support can be changed by pre-treating the surface, however its impact on electrodeposition of Cu remains unexplored [31, 32]. In this paper, mild conditions (lower concentrations of acid/base and temperature) will be maintained, in order to achieve a sufficiently hydrophilic GDE for deposition while at the same time avoiding GDE degradation. For this purpose, HNO_3 was investigated as the acid of choice as it seemed to work best (beneficial impact on surface properties while maintaining GDE structure) [31, 33–36].

The aim of this work is to synthesize Cu nanoparticles on rough surfaces, more specifically, a GDE electrode by using a dual pulse method. Here, for the first time, dual pulse electrodeposition is applied to deposit Cu on a GDE in methane sulfonic acid (MSA) electrolyte. The impact of the GDE pre-treatment on the size and morphology of the nanoparticles is investigated. After selecting the ideal pre-treatment, the effect of the dual pulse parameters on the size and distribution will be investigated on the pre-treated GDE. Finally, its stability under electrochemical conditions is compared to spray-painted Cu GDEs. This work can contribute significant to latest research concerning electrodeposition of metallic nanoparticles on rough surfaces. The electrodeposition of Cu done in this research can lead to new insides into the behavior of metallic nanoparticles on rough surface such as GDE.

2 Experimental

2.1 Chemicals

Copper sulfate pentahydrate ($CuSO_4.5H_2O$, 99 %) was purchased from Riedel-de Haën. Methane sulfonic acid (MSA, 70 % aq. sol.) was purchased from Alfa Aesar. Triton ® X-100 (TX100) was purchased from Acros organics. Nitric acid (HNO_3, 70 % aq. sol.) and sodium hydroxide (NaOH, pellets) are purchased from Chem-lab and Sigma-Aldrich, respectively. All solutions were prepared in ultra-pure water (MQ, Milli-Q grade, 18.2 MΩ cm) and purged with argon prior to deposition.

2.2 Electrochemical set-up

The electrodeposition of Cu was performed in a 4-electrode set-up, where a working electrode (WE, 4 cm2) consisting of carbon paper (Toray paper) was placed in between 2 counter electrodes (CE, 8 cm2) made of carbon paper (Sigracet ® 39 AA). Next to the WE, a saturated Ag/AgCl reference electrode (RE) is positioned. The measurements were performed with a Bio-logic VSP-300. All potentials applied in the experiments were derived from cyclic voltammetry (CV) measurements.

2.3 Preparation of the GDE

Before the synthesis of Cu on GDE, a surface modification of the GDE was interposed to ensure a higher hydrophilicity and thus an easier deposition. To this end, the GDEs were treated with either MQ, 0.1 M acid (HNO_3), 0.1 M base (NaOH) or 10 mM surfactant (TX100) for 24 h at room temperature after which the proper surface treatment was selected for further experiments. The GDEs were washed for 5 min, 3 min and 1 min with MQ and dried in a desiccator.

The dual pulse (Figure S1) experiments, which consists of 2 consecutive pulses, were carried out in a solution containing 10 mM $CuSO_4$ (as often used in literature [37–39]) and 2 M methane sulfonic acid (MSA) (essential to maintain an acidic environment to avoid Cu oxidation and an eco-friendly alternative for the commonly used H_2SO_4, i.e. reduced toxicity and biodegradable [17, 40–43]). In the first pulse, the nucleation pulse, the potential is stepped from open circuit potential (OCP, where no reaction occurs) to a potential negative enough to deposit Cu nuclei onto a substrate. In a second pulse, called the growth pulse, the nuclei of the first pulse grow at a potential more positive to the first one (resulting in less driving force), which inhibit the formation of new nuclei. Besides using TX100 during the pre-treatment of the GDE, it can also be added to the deposition solution of Cu. The addition of TX100 into the deposition solution, results in the deposition of Cu inside the GDE.

Once the optimal pre-treatment was selected, the impact of the deposition parameters, both the nucleation pulse as well as the growth pulse parameters were altered, to investigate their impact on the resulting material. At first, the nucleation potential (E_n) was varied between -0.5 V and -1 V. The nucleation charge (Q_n) was kept constant at -28.2 mC (≈ nucleation time of 1 s). The growth potential (E_g) and growth charge (Q_g) were altered between 0.05 V and 0.1 V and -67.5 mC, -135 mC and -270 mC, respectively.

2.4 Electrochemical and electrode surface analysis

Differences in pre-treatment of the GDE on the Cu electrodeposition mechanism were first analyzed with cyclic voltammetry (CV), within a potential range of -0.7 V and 0.7 V, with a scan rate of 50 mV s-1. Next, the nucleation mechanism of the Cu electrodeposition on pre-treated GDEs was studied using chronoamperometric experiments. The potential was stepped from the open circuit potential (OCP) to -0.3 V with a charge of 2.18 C. Both experiments were performed in a solution containing 0.1 M $CuSO_4$ and 2 M MSA.

Additionally, the point of zero charge of the GDEs was determined after pre-treatment using the pH drift method, also called the solid addition method[44]. This allowed us to determine whether the surfaces were positively or negatively charged, which led to a possible explanation of the shift in the CV curves. To this end, solutions of 5 mL of 0.01M NaCl were bubbled with argon to remove the dissolved CO_2. The pH of the solutions was adjusted between 6 and 11 with an increment of 1 using 0.01 M HCl and NaOH. An amount of 15 mg of pre-treated carbon paper was added and the solution was stirred for 24 h. The final pH was plotted against the initial pH. The intersection point of this curve with the reference curve is considered the point of zero charge. The reference curve is a straight line where final pH and initial pH coincide.

An FTIR spectrum of the TX100 pre-treated GDE was recorded between a wavelength of 399 cm-1 and 4000 cm-1. The GDE used was pre-treated with a 0.05 M TX100 at 80°C. This was necessary because the GDE needed to be crunched, mixed with KBr and pressed into a tablet.

The electrochemical active surface area (EASA) was calculated by performing capacitance measurements using cyclic voltammetry. GDE3 was used as an example of the dual pulse technique. As benchmark single pulse electrodeposition was used to calculate the relative EASA and was performed in a 10 mM $CuSO_4$ and 2 M MSA solution (purged with Ar) applying -0.5 V vs. Ag/AgCl sat. to deposit a loading of -0.096 C. Different CV measurements were performed at scan rates going from 150 mV s-1 to 25 mV s-1 with an increment of 25 mV s-1 with a potential range of ± 40 mV vs. OCP. A blank measurement was performed to eliminate the effect of the rough GDE surface. The experiment is also performed on the GDE before depositing any Cu to eliminate the difference in capacitive current between different GDE electrodes. The current obtained during this experiment is subtracted from the measured current after depositing Cu onto the GDE. Hereafter the current at OCP (of the second cycle) was plotted against the scan rate. The slope of the trendline is a measure of the EASA.

Surface morphology and changes in particle size were studied with a scanning electron microscope (SEM, FEI Quanta 250) at 5 kV using secondary electrons.

2.5 Stability test

The stability of electrodeposited Cu on the GDE surface, with a loading of 0.18 mg cm-2, was tested by applying a constant potential of -1.0 V vs RHE for 4 h in a solution of 0.5 M $KHCO_3$ (saturated with CO_2), using an H-type cell at room temperature. These results were compared to spray-painted Cu on GDE, with a loading of 0.2 mg cm-2. Cu was spray-painted using a solution of Cu (Sigma Aldrich 14-25 µm) and isopropanol (IPA).

The samples were diluted 10 times and adjusted to 1 % HNO_3 (Merck, Suprapur). The acidic solutions were analyzed via inductive coupled plasma mass spectrometry (ICP-MS, Agilent 7500).

3 Results and discussion

3.1 Influence of the pre-treatment of GDE

Figure 1 shows the first cycle of the CV experiments for the HNO_3, MQ, NaOH and TX100 pre-treatments. Shifts in the peak potential of Cu are observed, which is a significant indication that the pre-treatment has an effect on the electrodeposition of Cu on GDE. The HNO_3, NaOH and TX100 pre-treatments can be compared to the MQ pre-treatment, which functions as benchmark. The use of HNO_3 results in a positive potential shift, from -0.28 V to -0.22 V, compared to MQ, due to the fact that carboxylic groups are present at the GDE surface after the acid treatment [30, 45, 46]. These groups enhance the surface hydrophilicity, leading to a smoother electrodeposition of Cu on these surfaces. For TX100, a negative shift (from -0.28 V to -0.34 V) is observed compared to MQ. NaOH has the same effect as TX100 and again a negative shift (from -0.28 V to -0.32 V) is found.

<Figure 1>

Surface pH measurements (Figure 2) indicate that when using NaOH and TX100, the point of zero charge is located at pH 8.0 and pH 7.8, respectively. The Cu deposition solution has a pH lower than 1, inducing a positively charged surface, which results in the repulsion of Cu-ions and thus explains the need for a more negative potential to initiate the deposition of metallic Cu. Comparing this to HNO_3, which has a surface pH of 2.7, we can conclude that the surface, in case of HNO_3, will have a less pronounced positive charge compaired to TX100 and NaOH. This obviously means that the copper ions will encounter less repulsion in this case, which confirms the results of the CV measurements, as they indicated that a less negative potential is necessary for HNO_3. To summarize, a positive shift in peak potential is observed when using HNO_3 compared to MQ because of the negatively charged surface of the GDE due to its pre-treatment as such attracting the Cu^{2+} ions . The negative shift of TX100 and NaOH can be explained by the more positively charged surface, which causes the repulsion of the positive

Cu-ions resulting in the need for a more negative potential to reduce Cu-ions to metallic Cu on the GDE surface.

<Figure 2>

In addition to electrodeposition potential also the current density at the peak potential is an important parameter since it is directly related to the amount of deposited Cu. When comparing these peak current densities for the different pre-treatments, it can be observed that HNO_3 displayed a threefold drop in current density with respect to MQ. In case of NaOH and TX100 only a twofold drop in current density was perceptible. These lower current densities might be caused by the functional groups present at the surface as they would slow down diffusion of Cu to the surface, thus resulting in a lower current compared to the MQ blank.

In case of NaOH and HNO_3, a shoulder is present on the anodic peak, which would be attributed to the desorption of Cu from the surface after specific adsorption of Cu-ions during the reduction peak. During the CV measurements, a nucleation loop (NL) is present in case of NaOH and TX100. The NL appears in the potential range where nucleation occurs and is characterized by a cross over between the forward and reversed scan and were the current in the reversed scan is higher (more negative) than in the forward scan [47]. This is a typical behavior for the deposition of metallic Cu nuclei on a foreign (in this case GDE) surface and indicates that the deposition of Cu is easier on the Cu nuclei than on the GDE substrate. The fact that only NaOH and TX100 exhibit such a NL is caused by its positively charged surface, which obviously repels the positive Cu ions. Once some Cu nuclei are formed deposition will become easier on this growing nuclei explaining this loop. For the HNO_3-treated GDE this NL is not found as the positive Cu ions are attracted to the negatively charged surface making its deposition favorable from the start of the experiment [48].

In order to get a better understanding of the change in morphology, we investigated the nucleation mechanism of the Cu electrodeposition using current-time transient curves. The potential was shifted from an initial value, where no electrodeposition occurred to a potential (-0.3 V) negative enough to induce the electrodeposition of Cu. Figure 3 shows the current-time transient curves of the Cu electrodeposition using the 4 pre-treatments of the GDEs. The current increases due to the charging of the double layer, the formation of extra nuclei and the increase in size of the nuclei, reaching a maximum in current. A maximum in current is reached within 1 s in case of HNO_3, NaOH and MQ. Using TX100, on the other hand, it took up to 3 s to reach a maximum in current. After this point, diffusion zones start to overlap (deposition rate slows down) which results in a reduced surface area, leading to a decrease in current because of the transition to planar diffusion of Cu-ions to the growing islands [49–51]. The difference observed for TX100 in comparison to the other 3 pre-treatments (longer time to maximum current) might indicate the existence of another (slower) nucleation mechanism for TX100, which will be elaborated later on [52].

<Figure 3>

To determine the nucleation mechanism, the current-time transient curves were normalized and compared to the Scharifker-Hills model [53] using equation (1) and (2). According to this model, the nucleation can occur either through an instantaneous process or through a progressive route. The following equations describe the nucleation process for 3D nucleation with crystal growth dominated by localized hemispherical diffusion.

$$\left(\frac{I}{I_m}\right)^2 = \frac{1.9542}{\frac{t}{t_m}}\left(1 - e^{-1.2564\frac{t}{t_m}}\right)^2 \text{(instantaneous nucleation)} \qquad (1)$$

$$\left(\frac{I}{I_m}\right)^2 = \frac{1.2254}{\frac{t}{t_m}}\left(1 - e^{-2.3367\frac{t}{t_m}}\right)^2 \text{(progressive nucleation)} \qquad (2)$$

Where I is the current, I_m is the maximum current, t is time and t_m is the time at the maximum current. As can be observed in Figure 4, the transients from the experimentally obtained curves for MQ, HNO_3 and NaOH are in good agreement with the theoretically calculated curve for instantaneous nucleation, although a small deviation for NaOH is observed. This means that for all 3 cases, the nucleation occurs immediately at the beginning of the electrodeposition and no new nuclei are formed during the rest of the experiment. The experimental curve of TX100 overlaps with the progressive model, meaning nucleation proceeds via progressive nucleation, where nuclei are progressively formed throughout the experiment, and thus nucleation also occurs at later stages during the electrodeposition. This can be explained as follows. During the TX100 pre-treatment, long carbon chains are adsorbed on the GDE surface. If we look at the FTIR spectrum of a TX100 pre-treated GDE in Figure S2, 2 peaks at 2870 cm-1 and 2960 cm-1 are observed indicating the presence of methyl groups. These methyl groups are present in the TX100 molecule at the end of the molecular structure thus proving the presence of TX100 at the GDE surface. These carbon chains could potentially block the surface, resulting in a slower diffusion of Cu to the surface. Consequently, not all Cu-ions, present in the diffusion layer, are instantly reduced to metallic Cu. At a high enough deposition time, the transient starts to approach the curve of instantaneous nucleation. At that point, diffusion zones are overlapping and the formation of new nuclei becomes impossible at these zones [54].

<Figure 4>

As evidenced by Figure 4, TX100 follows another nucleation mechanism than HNO_3, MQ and NaOH. This is caused by steric hindrance and manifests itself in the growth of alternate morphologies as clearly visible in the SEM images (Figure 5). Major changes are perceived between TX100 and the other pre-treatments which results in the electrodeposition of hemispherical particles (1.7 µm ± 0.04 µm, Figure S3 D), consisting of smaller cubic shaped particles (200 nm) as opposed to the spherical shaped particles which were observed for the

other pre-treatments. It is clear that the use of TX100 limits the growth in certain directions by blocking certain facets from growing and at the same time promoting the growth of those facets that are not limited by the presence of TX100. This in turn results in the production of specifically shaped particles, or in this case where the growth of cubes is promoted.

In conclusion, while it is clear that TX100 results in a different, progressive, nucleation mechanism the rationale between this behavior is not as clear. In our opinion, this can have two potential causes. First, as already mentioned before by slowing down the diffusion of Cu to the substrate, it can be expected that the formation of nuclei is also delayed when using TX100. Second, and more hypothetical, it is possible that the growth facets, which are blocked from growing by TX100, allow a slower nucleation and thus lead to the progressive process.

On the contrary, only small changes in morphology exist between the pre-treatments with MQ (0.8 µm ± 0.02 µm, Figure S3 B), HNO_3 (1.0 µm ± 0.02 µm, Figure S3 A) and NaOH (1.8 µm ± 0.06 µm, Figure S3 C), which all proceed through instantaneous nucleation. The particle size using MQ varies slightly compared to HNO_3. The latter gives rise to a more uniform and dense particle distribution. Even more so, it allows deposition of particles on the inner matrix just beneath the surface of the GDE thus results in a better coverage and bigger (active) surface area (Figure S4 and Figure S5).

In addition to lower overvoltage requirement, the particles obtained using HNO_3 appear rougher compared to MQ treatment, resulting in an increased surface area which is beneficial for catalytic purposes.

<Figure 5>

Since the pre-treatment with HNO_3 gives rise to a more homogeneous particle distribution with an increased particle roughness, it was selected as the most optimal pre-treatment and will be

further used to investigate the impact of the deposition parameters on the Cu size and distribution.

3.2 Dual pulse electrodeposition of Cu on HNO_3 pre-treated GDE

In the first stages of growth it is plausible that the nuclei, formed in the preceding step, grow independently of each other. When this growth evolves, nuclei start to become bigger nanoparticles which eventually can result in the overlap of the diffusion zones of the particles, meaning the particles can no longer grow freely in all directions and will start agglomerating.

The influence of the nucleation potential on the particle size and the particle density is shown in Figure 6 (A and C). Upon increasing the nucleation potential, more energy is entering the system and more nuclei are deposited at the same time, leading to greater particle density [37, [49, 55, 56]. More particles are deposited so the available amount of energy needs to be divided between them, leading to smaller particles. It is clear that the particle density and their size on the electrode surface depend on the nucleation pulse.

<Table 1>

Comparing GDE1 with GDE2 and GDE4 to GDE6, the average size of the Cu particles is 148 nm (Figure S6 A), 91 nm (Figure S6 B), 136 nm (Figure S6 D) and 55 nm (Figure S6 F), respectively. This indicates that the particle size decreases with the nucleation potential. Histograms of GDE1, GDE4 exhibit 2 maxima. This has to do with ability of the particles to aggregate. Small nuclei which are within a specific radius attract each other, forming first order agglomerates. These same nuclei can also be attracted toward larger agglomerates, leading to a different particle size [57]. In addition, a higher particle density was observed with a negative increment of the nucleation potential (-0.75 V and -1 V compared to -0.5 V), which partially validates the smaller particle size as the same loading was deposited. Another possible cause for the smaller size is the theory of nucleation and growth of nuclei. This theory states that the radius of a particle is inversely proportional to the nucleation overpotential, meaning more

negative nucleation potentials lead to a smaller radius of the nuclei. This is related with the critical nuclei radius, which is larger when using less negative nucleation potentials. As such at more negative potentials, more nuclei will meet the required critical size leading to a higher particle density (and thus smaller particles) on the surface [55, 58]. Smaller nanoparticles are thus obtained using more negative nucleation potentials [59].

<Figure 6>

From Figure 7 it is clear that the size of the Cu particles alters with the growth charge. Considering GDE1, GDE3 and GDE4, the mean radius of the particles enlarged with increasing growth charge. This is straightforward considering that the growth charge is proportional to the duration of the experiment. At larger growth charge, the particles are given more time and energy to grow, ultimately resulting in bigger particles. Using deposition parameters of GDE3, a particle size of 45 nm (Figure S6 C) was obtained, which increased up to 148 nm for GDE1, because of the smaller growth potential (and thus larger growth charge) employed, favoring copper ions to deposit on preformed Cu islands.

<Figure 7>

The mean particle size decreases with an elevation in growth potential, as shown in Figure 8. The mean radius of GDE5 and GDE6 decreases from 61 nm (Figure S6 E) to 54 nm, respectively. These experiments were performed using the same growth charge. If we look at the deposition time required to perform these experiments, it shows that using a less negative growth potential, a longer time was needed to deposit the same amount of charge. This would thus mean that by depositing the Cu nanoparticles for the same duration, the nanoparticles will be using -0.05 V compared to -0.1 V. The growth potential is linked to the growth rate. A more negative potential leads to a higher growth rate, which means particles grow faster and during

the same amount of time, the particles will thus grow larger as compared to applying a less negative growth potential.

<Figure 8>

Using dual pulse leads to a better control in the electrodeposition of nanoparticles and smaller nanoparticles can be obtained compared to single pulse electrodeposition. This leads to an increased activity of the catalyst. To substantiate this assumption, the EASA of the nanoparticles deposited using single and dual pulse electrodeposition are compared. CV measurements are performed in a range ± 40 mV s-1 vs. OCP to make sure no faradaic contribution would be present during the experiment and only a capacitive current was measured. The scan rate varies from 150 mV s-1 to 25 mV s-1 with an increment of 25 mV s-1. The difference in current at OCP of the second scan is plotted against the scan rate in Figure 9. The slope of the trendline using single pulse is 10 times smaller than the slope of the dual pulse technique. Since the slope is an indication of the EASA of the deposited Cu nanoparticles, we can conclude that using dual pulse electrodeposition a bigger surface area is obtained, which will lead to higher activity of the catalyst.

<Figure 9>

As well-known in literature, the particle size of Cu, deposited on GC, can vary from the nanometer scale [60, 61] to the micrometer range [62]. In this paper we were able to control the particle size within the same range as literature states for the electrodeposition of Cu on GC, only we are using a rough surface. This has the advantage of increasing the active surface area and by doing so, higher current densities can be obtained.

All dual pulse parameters tested in this research have their own effect on the particle size and the particle distribution. The same trends were observed performing dual pulse electrodeposition of Cu on glassy carbon (smooth substrate). From reproducibility tests (Figure

S7), it is clear that another parameter, namely the constantly changing surface, plays an important role. This means, because of the rough surface of the GDE, the substrate is not always exactly the same, meaning it is difficult to deposit the particles with the same size upon reproduction. Nevertheless, this research opens perspectives about the electrodeposition of Cu onto rough surfaces. From this research it is clear the effect of the surface cannot be neglected and has to be taken into account.

3.3 Stability tests of Cu/GDE

Cu and its oxides are often used as electrocatalysts for CO_2 reduction because of their ability to convert it to higher value added chemicals such as methane and ethylene[8, 15]. This explains why the stability experiments for the Cu/GDE's, synthesized through electrodeposition and spray-painting, were tested under conditions often used in literature when investigating the CO_2 reduction. A potential of -1 V vs. RHE was applied for 4 h in a CO_2-saturated electrolyte containing 0.5 M $KHCO_3$. The electrolyte was tested with the ICP-MS for Cu suggesting possible detachment of Cu and thence instability of the electrocatalyst. When calculating the loss of Cu for the electrodeposited and the spray-painted Cu, 0.16 % and 0.72 % of Cu detached from the surface, respectively. This enables us to conclude that almost no Cu was present in the solution, thus suggesting they were both stable for 4 h under working conditions. However, when compared to each other, the percentage of Cu detaching from the surface when using the electrodeposited Cu was 22 % lower than spray-painted Cu.

<Figure 10>

During the first minutes of the experiment, using spray-painted Cu, the current decreases (to more positive values) drastically, as shown in Figure 10. After 30 min, an extreme current increase (to more negative currents) was observed. A possible hypothesis is that the Cu detaches during the first minutes of the experiment and redeposits after 30 min. This explains the fluctuating graph at the beginning of the experiment.

The reason for the detachment in both cases lays in the production of gaseous during the experiment, which is visible at the GDE surface. The detachment of Cu in regard to the spray-painted Cu was larger since it is not chemically bonded to the surface of the GDE as it was for electrodeposited Cu. This also explains the sudden drop during the first period of the experiment. Once the detached Cu was redeposited, the current was more stable.

4 Conclusion

Pre-treating the GDE is of utmost importance indeed, depending on the pre-treatment, differences in peak potential and nucleation mode were observed. As compared to MQ, TX100 and NaOH exhibit a negative peak potential shift while HNO_3 results in a positive shift. This was ascribed to a difference in surface charge: positive for TX100 and NaOH and negative for HNO_3. Additionally, TX100 also showed a different nucleation mode (progressive vs. instantaneous for the other 3), resulting in hemispherical particles, consisting of smaller cubic shaped particles.

Because of the rough surface of the GDEs, it was more difficult to control the electrodeposition of Cu. Reverting to dual pulse is necessary in order to obtain a better control because of the possibility to adjust more parameters. Here, increasing the nucleation potential (making it more negative) led to a higher particle density which caused the radius of the Cu particles to decrease. By increasing the growth potential or growth charge, larger particles were obtained. The Cu particles enlarged when applying a greater growth charge. Understanding the behavior of the deposition of Cu on GDE enables us to synthesize particles of any size which can be used for catalytic purposes.

Stability measurements showed that the electrodeposited Cu was more stable because of the chemical bonding between the Cu and the GDE along with the fact that it can be deposited onto the inner matrix of the GDE carbon fibers, which means they will less easily detach. This in

comparison with the spray-painted Cu, which detached during the first few minutes of the experiment and afterwards redeposited on the GDE resulting in a chemical bond between them.

Considering the importance of the pre-treatment of the GDE and changes in particle size in the dual pulse parameter tests, this research is of great importance in unraveling the behavior of Cu electrodeposition on rough surfaces. This work will also contribute to future research that will be conducted on electrodeposition on rough surfaces.

5 Declarations

5.1 Funding

L. Pacquets was supported through a PhD fellowship strategic basic research (1S56918N) of the Research Foundation – Flanders (FWO). N. Daems was supported through a postdoctoral fellowship (12Y3919N – ND) of the Research Foundation – Flanders (FWO). S. Neukermans was supported through an FWO project grant (G093317N). This research was financed by the research counsel of the university of Antwerp (BOF-GOA 33928). The authors recognize the contribution of Thomas Kenis for analytical validation and methodology.

5.2 Conflicts of interest

Not applicable

5.3 Availability of data

Not applicable

5.4 Code availability

Not applicable

5.5 Authors contribution

All authors contributed significantly to this work.

6 Bibliography

[1] D. Kim, C. S. Kley, Y. Li, and P. Yang, “Copper nanoparticle ensembles for selective electroreduction of CO_2 to $C_2 – C_3$ products,” *Proc. Natl. Acad. Sci.*, vol. 114, no. 40, pp. 10560–10565, 2017.

[2] R. Reske, H. Mistry, F. Behafarid, B. R. Cuenya, and P. Strasser, “Particle Size Effects

in the Catalytic Electroreduction of CO_2 on Cu Nanoparticles," *J Amer Chem Soc*, vol. 136, no. 3, pp. 6978–6986, 2014.

[3] H. J. Yang, S. Y. He, H. L. Chen, and H. Y. Tuan, "Monodisperse copper nanocubes: Synthesis, self-assembly, and large-area dense-packed films," *Chem. Mater.*, vol. 26, no. 5, pp. 1785–1793, 2014.

[4] K. D. Yang, "Morphology-Directed Selective Production of Ethylene or Ethane from CO2 on a Cu Mesopore Electrode," *Angew. Chemie*, 2016.

[5] A. Tamilvanan, K. Balamurugan, K. Ponappa, and B. M. Kumar, "Copper Nanoparticles: Synthetic Strategies, Properties and Multifunctional Application," *Int. J. Nanosci.*, vol. 13, no. 02, p. 1430001, 2014.

[6] Y. Lee, J. Choi, K. J. Lee, N. E. Stott, and D. Kim, "Large-scale synthesis of copper nanoparticles by chemically controlled reduction for applications of inkjet-printed electronics," *Nanotechnology*, vol. 19, no. 41, p. 415604, 2008.

[7] Z. Yaghoubi, "Selecting nanoparticles in the medical industry based upon AHP method," vol. 6, no. 1, pp. 45–54, 2015.

[8] O.A. Baturina, "CO_2 electroreduction to hydrocarbons on carbon-supported Cu nanoparticles.," pp. 5–6, 2008.

[9] H. S. Jeon *et al.*, "Prism-shaped Cu nanocatalysts for electrochemical CO reduction to ethylene," 2017.

[10] A. Loiudice *et al.*, "Tailoring Copper Nanocrystals towards C_2 Products in Electrochemical CO_2 Reduction Angewandte," vol. 94720, pp. 5789–5792, 2016.

[11] W. Y. Ko, W. H. Chen, C. Y. Cheng, and K. J. Lin, "Architectural growth of Cu nanoparticles through electrodeposition," *Nanoscale Res. Lett.*, vol. 4, no. 12, pp.

1481–1485, 2009.

[12] T. Y. Chang, R. M. Liang, P. W. Wu, J. Y. Chen, and Y. C. Hsieh, “Electrochemical reduction of CO_2 by Cu_2O-catalyzed carbon clothes,” *Mater. Lett.*, vol. 63, no. 12, pp. 1001–1003, 2009.

[13] M. T. H. Le, “Electrochemical Reduction of CO_2 to Methanol,” vol. 152, no. August, pp. 1–97, 2011.

[14] K. Malik, N. K. Bajaj, and A. Verma, “Effect of catalyst layer on electrochemical reduction of carbon dioxide using different morphologies of copper,” *J. CO2 Util.*, vol. 27, no. June, pp. 355–365, 2018.

[15] R. Kas, R. Kortlever, H. Yilmaz, M. T. M. Koper, and G. Mul, “Manipulating the Hydrocarbon Selectivity of Copper Nanoparticles in CO_2 Electroreduction by Process Conditions,” *ChemElectroChem*, vol. 2, no. 3, pp. 354–358, 2015.

[16] W. Tang *et al.*, “The importance of surface morphology in controlling the selectivity of polycrystalline copper for CO_2 electroreduction,” *Phys. Chem. Chem. Phys.*, vol. 14, no. 1, pp. 76–81, 2012.

[17] H. Cao, T. Hang, H. Ling, and M. Li, “Behaviors of Chloride Ions in Methanesulfonic Acid Bath for Copper Electrodeposition of Through-Silicon-Via,” *J. Electrochem. Soc.*, vol. 160, no. 4, pp. D146–D149, 2013.

[18] K. Manthiram, B. J. Beberwyck, and A. P. Alivisatos, “Enhanced electrochemical methanation of carbon dioxide with a dispersible nanoscale copper catalyst,” *J. Am. Chem. Soc.*, vol. 136, no. 38, pp. 13319–13325, 2014.

[19] A. E. W. Horst, K. M. Mangold, and D. Holtmann, “Application of gas diffusion electrodes in bioelectrochemical syntheses and energy conversion,” *Biotechnol.*

Bioeng., vol. 113, no. 2, pp. 260–267, 2016.

[20] A. Kaisheva, I. Iliev, R. Kazareva, S. Christov, U. Wollenberger, and F. W. Scheller, "Enzyme/gas-diffusion electrodes for determination of phenol," *Sensors Actuators, B Chem.*, vol. 33, no. 1–3, pp. 39–43, 1996.

[21] I. Merino-Garcia, J. Albo, and A. Irabien, "Tailoring gas-phase CO_2 electroreduction selectivity to hydrocarbons at Cu nanoparticles," *Nanotechnology*, vol. 29, no. 1, p. 14001, 2018.

[22] N. S. Romero Cuellar, K. Wiesner-Fleischer, M. Fleischer, A. Rucki, and O. Hinrichsen, "Advantages of CO over CO_2 as reactant for electrochemical reduction to ethylene, ethanol and n-propanol on gas diffusion electrodes at high current densities," *Electrochim. Acta*, vol. 307, pp. 164–175, 2019.

[23] Y. L. Qiu, H. X. Zhong, T. T. Zhang, W. Bin Xu, X. F. Li, and H. M. Zhang, "Copper Electrode Fabricated via Pulse Electrodeposition: Toward High Methane Selectivity and Activity for CO_2 Electroreduction," *ACS Catal.*, vol. 7, no. 9, pp. 6302–6310, 2017.

[24] H. Guo *et al.*, "Controllable synthesis of Cu–Ni core–shell nanoparticles and nanowires with tunable magnetic properties," *Chem. Commun.*, vol. 52, no. 42, pp. 6918–6921, 2016.

[25] K. R. Lee, J. H. Lim, J. K. Lee, and H. S. Chun, "Reduction of Carbon Dioxide in 3-Dimensional Gas Diffusion Electrodes," *Korean J. Chem. Eng.*, vol. 16, no. 6, pp. 829–836, 1999.

[26] H. Xiang, S. Rasul, K. Scott, J. Portoles, P. Cumpson, and E. H. Yu, "Enhanced selectivity of carbonaceous products from electrochemical reduction of CO_2 in aqueous

media," *J. CO2 Util.*, vol. 30, no. December 2018, pp. 214–221, 2019.

[27] S. Sen *et al.*, "Pulse Plating of Copper Nanostructures onto Gas Diffusion Layers for the Electroreduction of Carbon Dioxide to Hydrocarbons," *2017 MRS Fall Meet. Exhib.*, 2017.

[28] C. Moreno-Castilla, F. Carrasco-Marín, F. J. Maldonado-Hódar, and J. Rivera-Utrilla, "Effects of non-oxidant and oxidant acid treatments on the surface properties of an activated carbon with very low ash content," *Carbon N. Y.*, vol. 36, no. 1–2, pp. 145–151, 1998.

[29] J. P. Chen and S. Wu, "Acid/Base-Treated Activated Carbons: Characterization of Functional Groups and Metal Adsorptive Properties," *Langmuir*, vol. 20, no. 6, pp. 2233–2242, 2004.

[30] L. Fan *et al.*, "Effects of surface modification on the reactivity of activated carbon in direct carbon fuel cells," *Electrochim. Acta*, vol. 284, pp. 630–638, 2018.

[31] A. E. Aksoylu, M. Madalena, A. Freitas, M. F. R. Pereira, and J. L. Figueiredo, "Effects of different activated carbon supports and support modifications on the properties of Pt/AC catalysts," *Carbon N. Y.*, vol. 39, no. 2, pp. 175–185, 2001.

[32] S. M. Senthil Kumar, J. Soler Herrero, S. Irusta, and K. Scott, "The effect of pretreatment of Vulcan XC-72R carbon on morphology and electrochemical oxygen reduction kinetics of supported Pd nano-particle in acidic electrolyte," *J. Electroanal. Chem.*, vol. 647, no. 2, pp. 211–221, 2010.

[33] J. Bai, X. Bo, D. Zhu, G. Wang, and L. Guo, "A comparison of the electrocatalytic activities of ordered mesoporous carbons treated with either HNO_3 or NaOH," *Electrochim. Acta*, vol. 56, no. 2, pp. 657–662, 2010.

[34] M. J. Lázaro, L. Calvillo, E. G. Bordejé, R. Moliner, R. Juan, and C. R. Ruiz, "Functionalization of ordered mesoporous carbons synthesized with SBA-15 silica as template," *Microporous Mesoporous Mater.*, vol. 103, no. 1–3, pp. 158–165, 2007.

[35] X. Wang, A. S. Varela, A. Bergmann, S. Kühl, and P. Strasser, "Catalyst Particle Density Controls Hydrocarbon Product Selectivity in CO2Electroreduction on CuOx," *ChemSusChem*, vol. 10, no. 22, pp. 4642–4649, 2017.

[36] J. Li, L. Ma, X. Li, C. Lu, and H. Liu, "Effect of nitric acid pretreatment on the properties of activated carbon and supported palladium catalysts," *Ind. Eng. Chem. Res.*, vol. 44, no. 15, pp. 5478–5482, 2005.

[37] R. L. Harniman, D. Plana, G. H. Carter, K. A. Bradley, M. J. Miles, and D. J. Fermín, "Real-time tracking of metal nucleation via local perturbation of hydration layers," *Nat. Commun.*, vol. 8, no. 1, 2017.

[38] M. Nagar, A. Radisic, K. Strubbe, and P. M. Vereecken, "The Effect of the Substrate Characteristics on the Electrochemical Nucleation and Growth of Copper," *J. Electrochem. Soc.*, vol. 163, no. 12, pp. D3053–D3061, 2016.

[39] W. Shao, G. Pattanaik, and G. Zangari, "Electrochemical Nucleation and Growth of Copper from Acidic Sulfate Electrolytes on n-Si(001)," *J. Electrochem. Soc.*, vol. 154, no. 7, p. D339, 2007.

[40] K. AOTANI and H. SUMIYA, "Studies on Electrodeposition of Copper from Methanesulphonic Acid Bath," *J. Met. Finish. Soc. Japan*, vol. 8, no. 1, pp. 12–18, 2011.

[41] M. D. Gernon, M. Wu, T. Buszta, and P. Janney, "Environmental benefits of methanesulfonic acid," *Green Chem.*, vol. 1, no. 3, pp. 127–140, 1999.

[42] S. Ki Cho, M. Jun Kim, and J. Jeong Kim, “MSA as a Supporting Electrolyte in Copper Electroplating for Filling of Damascene Trenches and Through Silicon Vias,” *Electrochem. Solid-State Lett.*, vol. 14, no. 5, p. D52, 2011.

[43] M. Hasan and J. F. Rohan, “Cu Electrodeposition from Methanesulfonate Electrolytes for ULSI and MEMS Applications,” *J. Electrochem. Soc.*, vol. 157, no. 5, p. D278, 2010.

[44] K. Singh, R. Bharose, S. K. Verma, and V. K. Singh, “Potential of powdered activatedmustard cake for decolorising raw sugar,” *J. Sci. Food Agric.*, vol. 93, no. 1, pp. 157–165, 2013.

[45] L. Thi Mai Hoa, “Characterization of multi-walled carbon nanotubes functionalized by a mixture of HNO_3/H_2SO_4,” *Diam. Relat. Mater.*, vol. 89, no. May, pp. 43–51, 2018.

[46] Y. C. Chiang, W. H. Lin, and Y. C. Chang, “The influence of treatment duration on multi-walled carbon nanotubes functionalized by H_2SO_4 /HNO_3 oxidation,” *Appl. Surf. Sci.*, vol. 257, no. 6, pp. 2401–2410, 2011.

[47] M. T. Pise, S. Srinivas, A. Chatterjee, B. P. Kashyap, R. N. Singh, and S. S. V. Tatiparti, “Influence of surface condition on the current densities rendering nucleation loop during cyclic voltammetry for electrodeposition of Pd thin films,” *Surfaces and Interfaces*, vol. 20, p. 100525, 2020.

[48] M. Rezaei, S. H. Tabaian, and D. F. Haghshenas, “A kinetic description of Pd electrodeposition under mixed control of charge transfer and diffusion,” *J. Electroanal. Chem.*, vol. 687, pp. 95–101, 2012.

[49] A. Radisic, F. M. Ross, and P. C. Searson, “In situ study of the growth kinetics of individual island electrodeposition of copper,” *J. Phys. Chem. B*, vol. 110, no. 15, pp.

7862–7868, 2006.

[50] S. Wu, Z. Yin, Q. He, G. Lu, Q. Yan, and H. Zhang, “Nucleation mechanism of electrochemical deposition of Cu on reduced graphene oxide electrodes,” *J. Phys. Chem. C*, vol. 115, no. 32, pp. 15973–15979, 2011.

[51] R. Tolosa, “Electrochemical Deposition Mechanism for ZnO Nanorods: Diffusion Coefficient and Growth Models,” *J. Electrochem. Soc.*, vol. 158, no. 11, pp. E107–E110, 2011.

[52] X. Zhou, Y. Wang, Z. Liang, and H. Jin, “Electrochemical deposition and nucleation/growth mechanism of Ni-Co-Y_2O_3 multiple coatings,” *Materials (Basel).*, vol. 11, no. 7, 2018.

[53] B. Scharifker, “Theoretical and experimental studies of multiple nucleation,” *Electrochim. Acta*, vol. 28, no. 7, pp. 879–889, 1982.

[54] G. Gunawardena, G. Hills, I. Montenegro, and B. Scharifker, “Electrochemical nucleation. Part I. General considerations,” *J. Electroanal. Chem.*, 1982.

[55] A. Pei, G. Zheng, F. Shi, Y. Li, and Y. Cui, “Nanoscale Nucleation and Growth of Electrodeposited Lithium Metal,” *Nano Lett.*, vol. 17, no. 2, pp. 1132–1139, 2017.

[56] B. Geboes, B. Vanrenterghem, J. Ustarroz, and D. Pauwels, “Influence of the Morphology of Electrodeposited Nanoparticles on the Activity of Organic Halide Reduction,” *Chem. Eng. Trans.*, vol. 41, pp. 73–78, 2014.

[57] J. Ustarroz, X. Ke, A. Hubin, S. Bals, and H. Terryn, “New Insights into the Early Stages of Nanoparticle Electrodeposition,” *J. Phys. Chem. C*, vol. 116, no. 3, pp. 2322–2329, 2012.

[58] D. R. Ely and R. E. García, “Heterogeneous Nucleation and Growth of Lithium

Electrodeposits on Negative Electrodes," *J. Electrochem. Soc.*, vol. 160, no. 4, pp. A662–A668, 2013.

[59] L. Huang, E. S. Lee, and K. B. Kim, "Electrodeposition of monodisperse copper nanoparticles on highly oriented pyrolytic graphite electrode with modulation potential method," *Colloids Surfaces A Physicochem. Eng. Asp.*, vol. 262, no. 1–3, pp. 125–131, 2005.

[60] Y. Oztekin *et al.*, "Copper nanoparticle modified carbon electrode for determination of dopamine," *Electrochim. Acta*, vol. 76, pp. 201–207, 2012.

[61] L. Xi, D. Shou, and F. Wang, "Electrodeposition of monodispersed Cu nanoparticles on poly-p-aminobenzene sulfonic acid functionalized glassy carbon electrode and the electrocatalytic reduction toward H2O2," *J. Electroanal. Chem.*, vol. 747, pp. 83–90, 2015.

[62] A. E. Bolzán, "Electrodeposition of copper on glassy carbon electrodes in the presence of picolinic acid," *Electrochim. Acta*, vol. 113, no. 2, pp. 706–718, 2013.

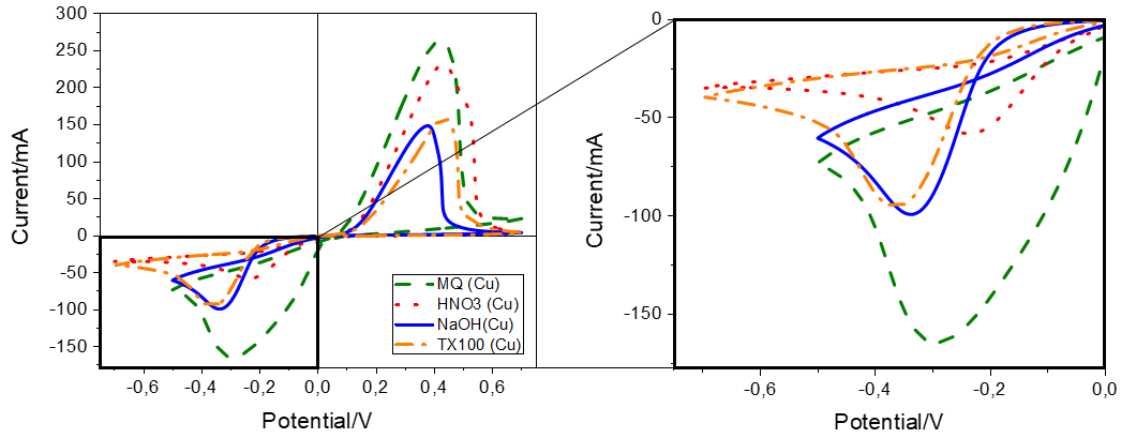

Figure 1: First cycle of CV measurements of MQ (dashed), HNO3 (dotted), NaOH (solid) and TX100 (dash dotted) treatment with a scan rate of 50 mV s-1 (potential are plotted vs Ag/AgCl saturated)

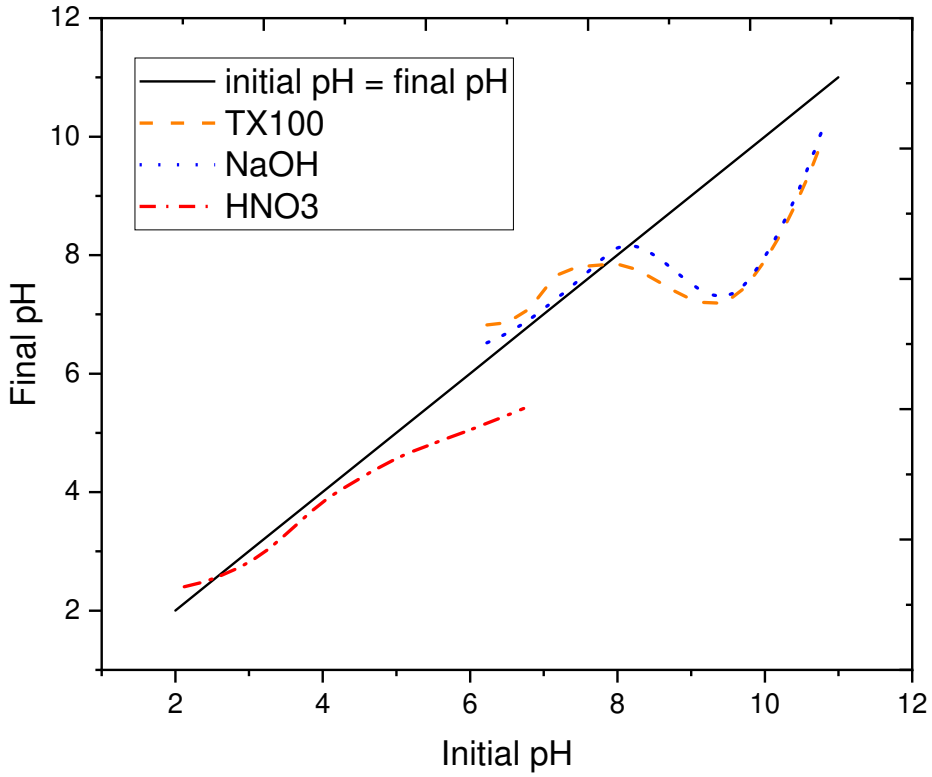

Figure 2: Determination of point of zero charge of TX100 (dashed), NaOH (dotted) and HNO_3 (dash dotted) pre-treated GDEs in a pH range of 2 to 11 with an increment of 1

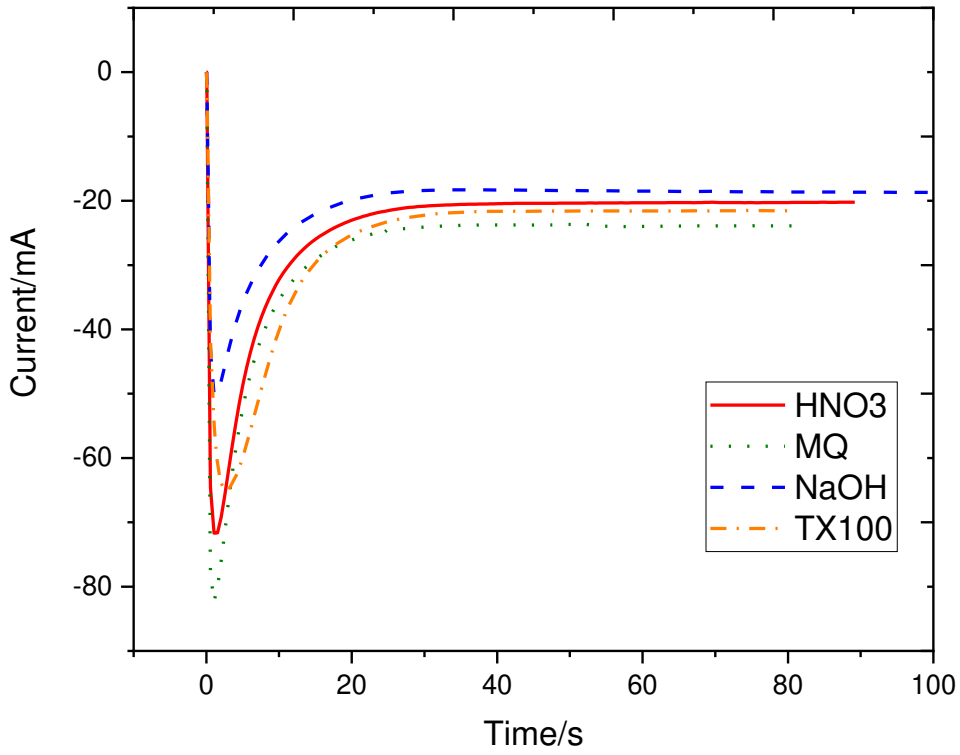

Figure 3: Current-time transient curves of Cu electrodeposition on HNO_3 (solid), MQ (dotted), NaOH (dashed) and TX100 (dash dotted) pre-treated GDE

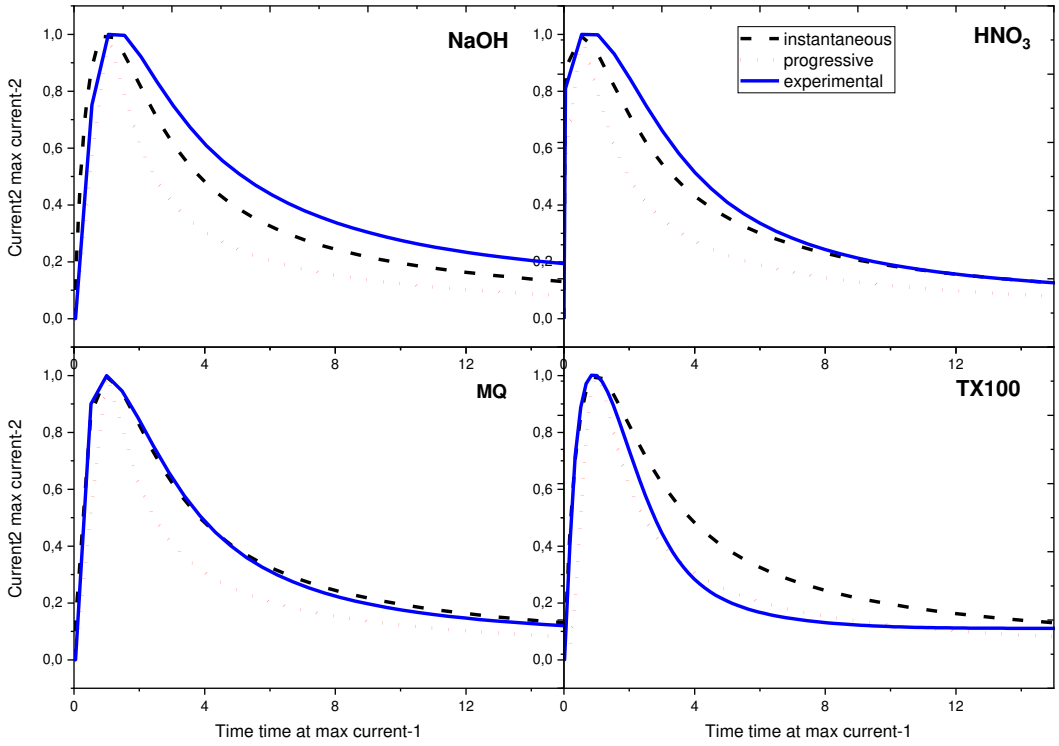

Figure 4: Non-dimensional I2 I_m-2 vs. t t_m-1 of the current-time transient curves, shown in Figure 3, compared to the theoretically calculated curve of instantaneous and progressive nucleation

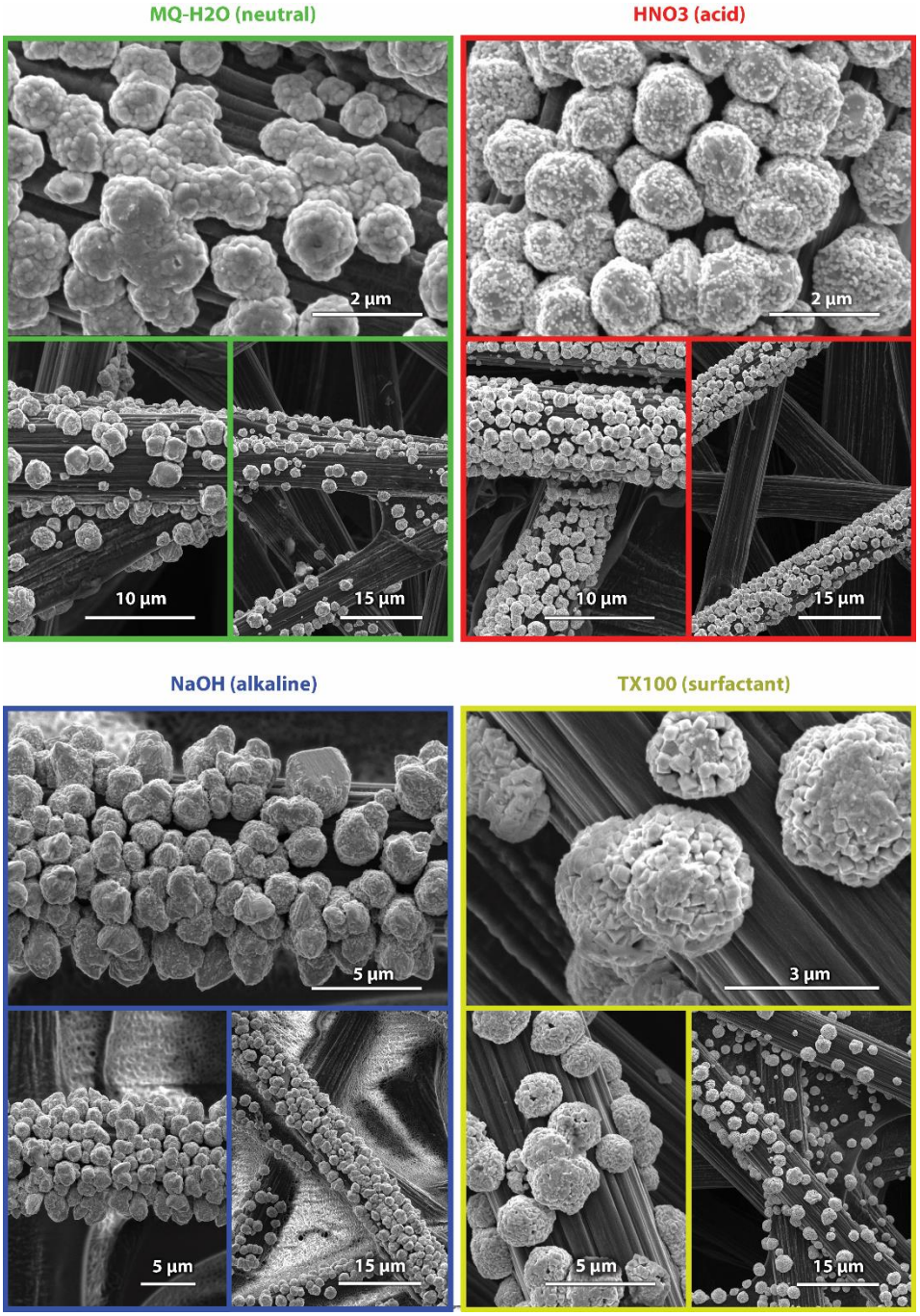

Figure 5: Impact of surface pre-treatment on the electrodeposition of copper particles: single pulse electrodeposited Cu on MQ (neutral); HNO_3 (acid); NaOH (alkaline); TX100 (surfactant) pre-treated GDEs

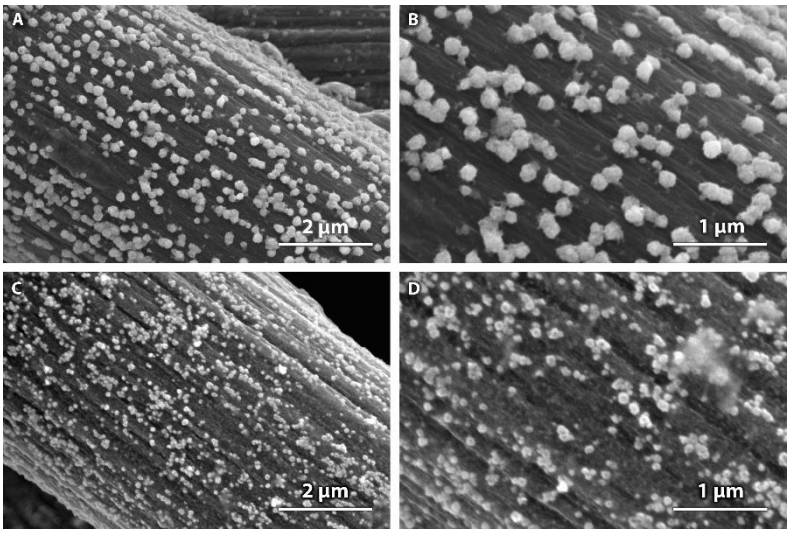

Figure 6: SEM images of Cu electrodeposition in MSA on GDE via dual pulse with different nucleation potentials (A, B) GDE1 and (C, D) GDE2

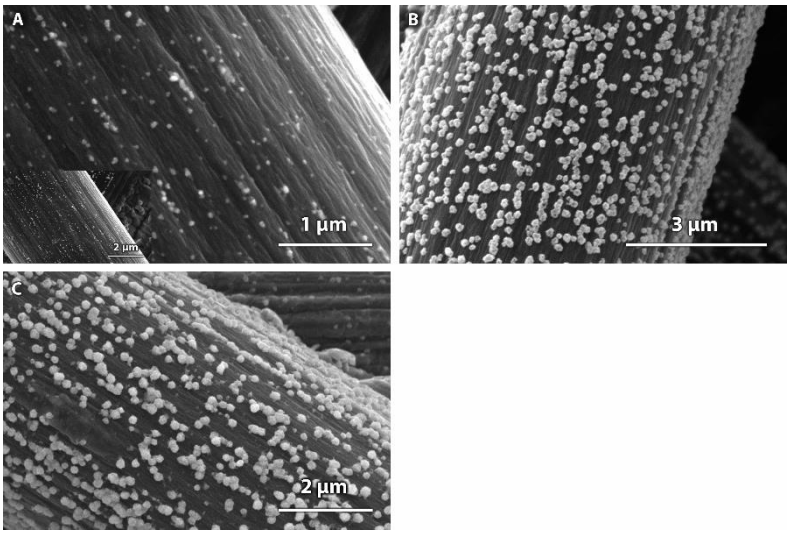

Figure 7: SEM images of Cu electrodeposition in MSA on GDE via dual pulse with varying growth charge (A) Q_g -0.0675 C, GDE3; (B) Q_g -0.135 C, GDE4 and (C) Q_g -0.270 C, GDE1

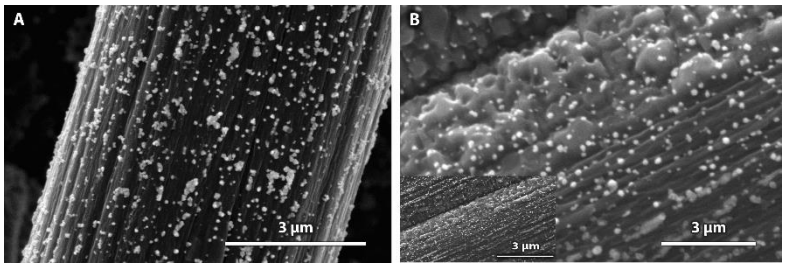

Figure 8: SEM images of Cu electrodeposition in MSA on GDE via dual pulse with different growth potentials (A) E_g -0.05 V, GDE5 and (B) E_g -0.1 V, GDE6

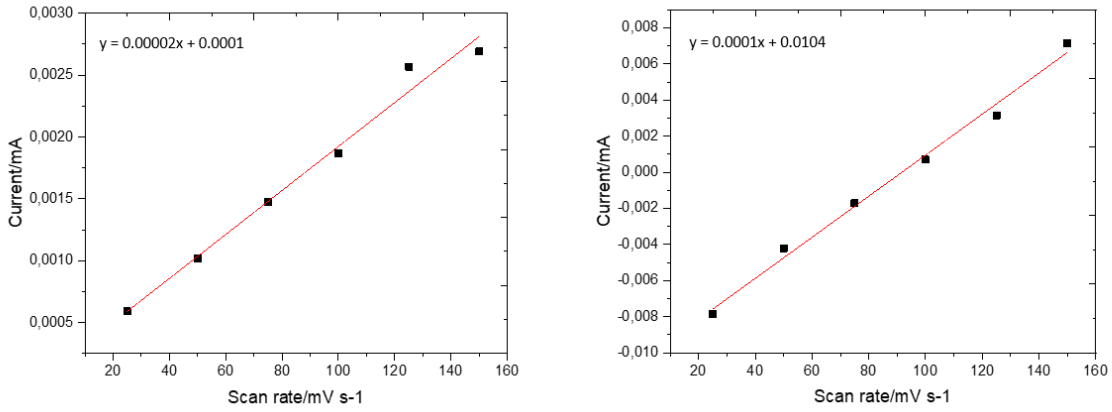

Figure 9: plot of capacitive current against scan rate (left) single pulse; (right) dual pulse electrodeposition in 0.1 M HClO4 with scan rates going from 150 mv s-1 to 25 mV s-1 with an increment of 25 mV s-1

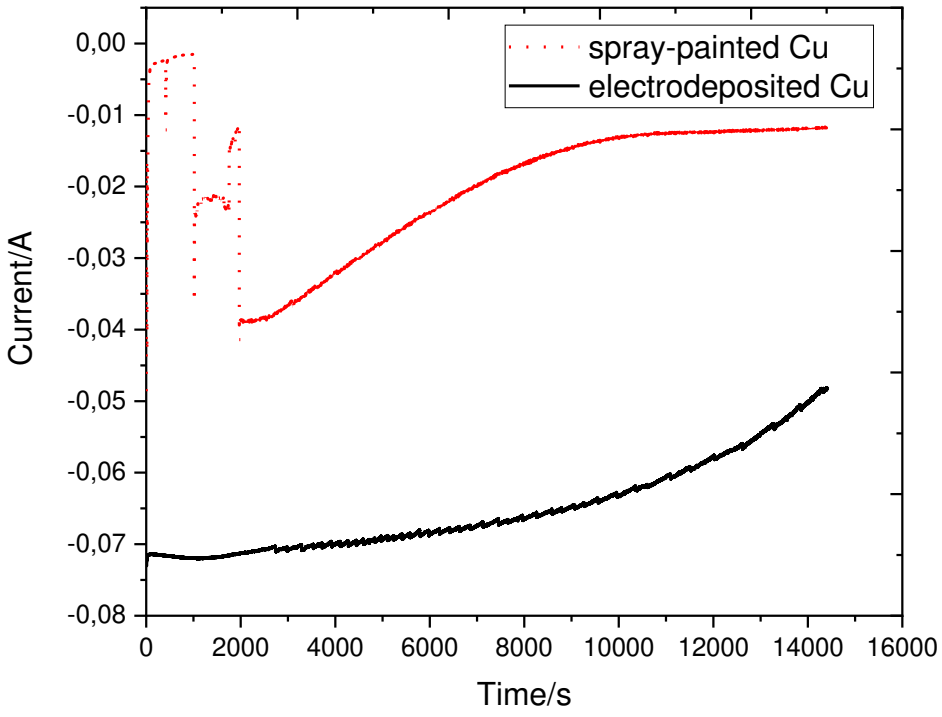

Figure 10: Current response for stability testing, comparing electrodeposited Cu (solid) and spray-painted Cu (dot) when applying -1 V vs. RHE using a CO_2 saturated electrolyte containing 0.5 M $KHCO_3$

Table 1: Deposition parameters for the dual pulse deposition of Cu in 10 mM $CuSO_4$ and 2 M MSA

Electrode number	Nucleation potential/V	Nucleation time/s	Growth potential/V	Growth charge/C	Particle size/nm
GDE1	-0.5	1	-0.1	-0.27	148 ± 3
GDE2	-0.75	1	-0.1	-0.27	91 ± 1
GDE3	-0.5	1	-0.1	-0.0675	45 ± 1
GDE4	-0.5	1	-0.1	-0.135	136 ± 3
GDE5	-1	1	-0.05	-0.135	61 ± 2
GDE6	-1	1	-0.1	-0.135	55 ± 1